Changes in the Red Sea Overturning Circulation during Marine Isotope Stage 3

Raphaël Hubert-Huard[1], Nils Andersen[2], Helge W. Arz[3], Werner Ehrmann[4], Gerhard Schmiedl[1]

[1]Institute for Geology, Universität Hamburg, Bundesstrasse 55, 20146 Hamburg, Germany
[2]Leibniz-Laboratory for Radiometric Dating and Stable Isotope Research, Christian-Albrechts-Universität zu Kiel, Max-Eyth-Strasse 11-13, 24118 Kiel, Germany
[3]Leibniz Institute for Baltic Sea Research Warnemünde, Seestrasse 15, 18119 Rostock-Warnemünde, Germany
[4]Institute of Geophysics and Geology, Universität Leipzig, Talstrasse 35, 04103 Leipzig, Germany

Correspondence to: Raphaël Hubert-Huard (raphael.hubert-huard@uni-hamburg.de)

Abstract. The oceanography of the Red Sea is controlled by the restricted exchange of water masses with the Indian Ocean and by high evaporation rates due to the arid climate of the surrounding land areas. In the northern Red Sea, the formation of oxygen-rich subsurface waters ventilates the deeper parts of the basin, but little is known about the variability of this process in the past. The stable oxygen and carbon isotope records of epibenthic foraminifera from a sediment core of the central Red Sea and comparison with existing isotope records allow for the reconstruction of changes in the Red Sea Overturning Circulation (ROC) during Marine Isotope Stage 3. The isotope records imply millennial-scale variations in the ROC, in phase with climate variability of the high northern latitudes. This suggests an immediate response of dense water formation to the regional climate and hydrology of the northern Red Sea. Deep-water formation was intensified under the influence of cold and hyper-arid conditions during Heinrich stadials and was diminished during Dansgaard-Oeschger interstadials. While these changes are reflected in both stable oxygen and carbon isotope records, the latter data also exhibit changes in phase with the African-Indian monsoon system. The decoupling of the stable carbon and oxygen isotope records at the summer monsoon maximum centred around 55–60 ka B.P. may be associated with an increased inflow of nutrient-rich intermediate waters from the Arabian Sea to the central Red Sea. This process fuelled local surface-water productivity resulting in enhanced remineralization of sinking organic matter and release of ^{12}C at intermediate water depths.

1 Introduction

The landlocked basin of the Red Sea is bordered by the semiarid to arid regions of the Arabian Peninsula and northern Africa (Fig. 1). The oceanography of the Red Sea is characterized by the restricted exchange with the Indian Ocean through the narrow and only 137 m deep Hanish sill of the Bab al-Mandab strait (Smeed, 1997, 2004). The exchange processes exhibit distinct seasonal contrasts, which are closely linked to the monsoonal wind system. During the NE monsoon in winter, a two-layer system prevails with inflowing surface waters from the Gulf of Aden and the deeper water mass outflow of Red Sea Water (RSW). During the summer SW monsoon, a three-layer system develops with outflowing surface waters and diminished RSW outflow, but the intrusion of nutrient-rich Gulf of Aden Intermediate Water (GAIW) (Smeed, 1997, 2004). Enhanced

evaporation rates result in high sea-surface salinities (SSS) with maximum values above 40 psu in the northern Red Sea. As a result, warm (21.6–21.8 °C) and saline (40.5–40.6 psu) intermediate and deep-water masses form in winter by cooling of
35   highly saline surface waters in the Gulfs of Suez and Aqaba, and occasionally in the northernmost open Red Sea (Cember, 1988; Eshel et al., 1994; Woelk and Quadfasel, 1996; Papadopoulos et al., 2015) (Fig. 2). As part of the Red Sea Overturning Circulation (ROC), the newly formed subsurface water masses extend southward and ventilate the deep-sea ecosystems, with estimated residence times of 40 to 90 years (Fig. 3) (Woelk and Quadfasel, 1996). Finally, RSW flows over the sill at Bab al-Mandab and spreads southward into the Indian Ocean along the African continental slope where it can be traced back to the
40   Agulhas Current (Roman and Lutjeharms, 2009).
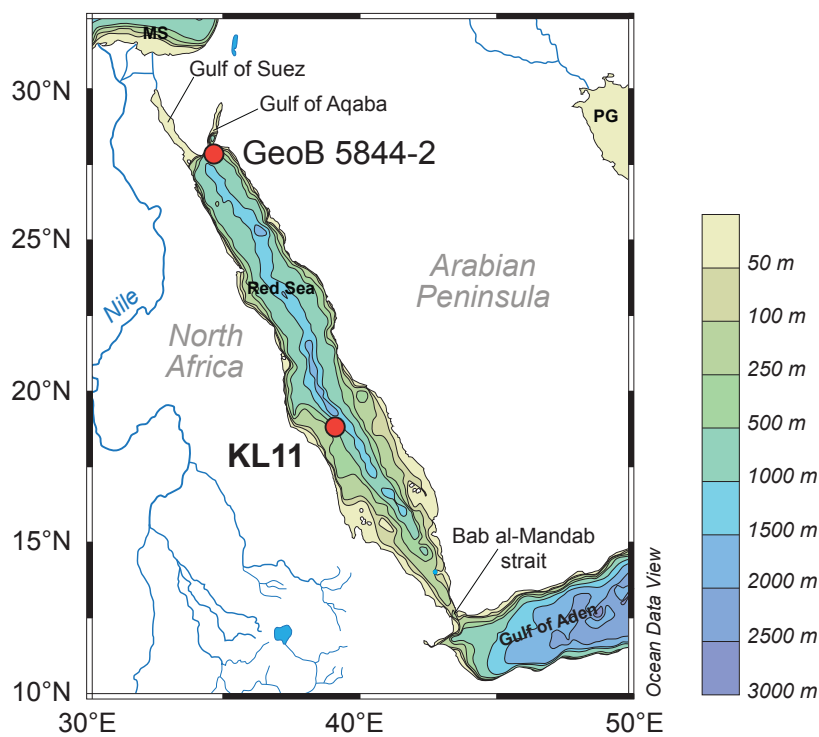
Figure 1. Bathymetric map of the Red Sea with the locations of core GeoTü KL11 investigated in this study and GeoB 5844-2 (Arz et al., 2007). Map generated with Ocean Data View (Schlitzer, 2015).

45
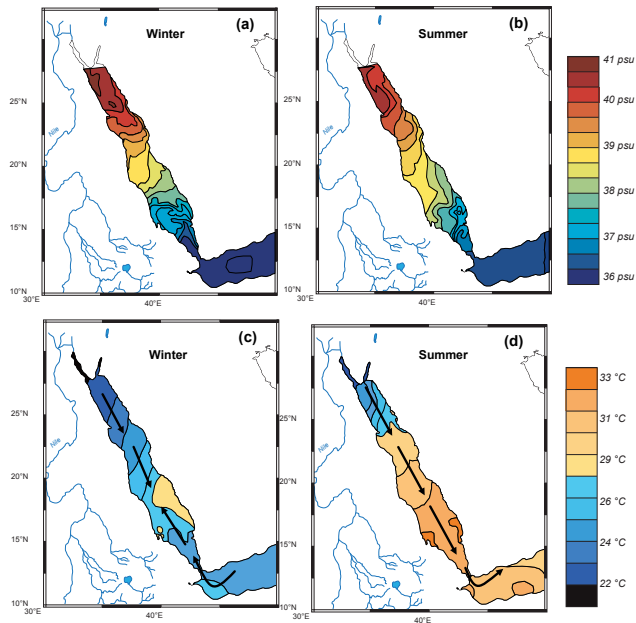
Figure 2. Seasonal sea-surface salinity distribution during the **(a)** winter (November – March) and the **(b)** summer (June – September) (Sofianos et al., 2003). Seasonal sea-surface temperature distribution and averaged net surface currents during the **(c)** winter (October – April) and the **(d)** summer (May – September) (Raitsos et al., 2013, 2015).

An oxygen minimum zone is developed below the oxygen-saturated surface layer, between approximately 200 and 700 m water depth (Sofianos and Johns, 2007). The most extreme oxygen deficiencies are restricted to the central and southern Red Sea basin, with oxygen concentrations as low as 10 µmol kg⁻¹ (~0.2 ml l⁻¹) (Fig. 3). The productivity in the surface water reveals regional and seasonal contrasts, with generally oligotrophic conditions in the central and northern Red Sea but meso- to eutrophic conditions south of 19° N (Raitsos et al., 2013). Maximum phytoplankton activity occurs during winter and is related to vertical mixing in the northern and central Red Sea and wind-induced horizontal intrusion of nutrient-rich water from the Gulf of Aden in the south (Naqvi et al., 1986; Eshel and Naik, 1997; Raitsos et al., 2013). Surface productivity is minimal during summer stratification in most areas of the Red Sea, but the intrusion of GAIW into the surface water results in phytoplankton blooms in the southern Red Sea (Dreano et al., 2016).
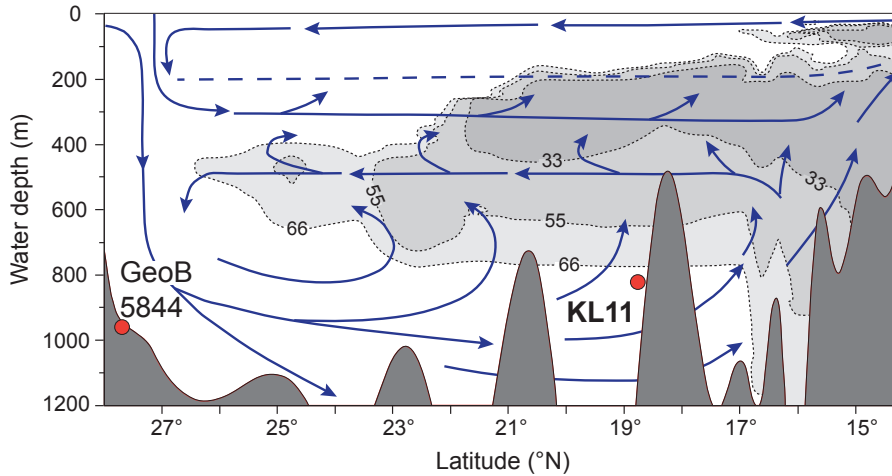
Figure 3. Generalized overturning circulation (blue arrows; Cember, 1988) and dissolved oxygen concentration (stippled lines and shadings; Sofianos and Johns, 2007) along a NNW-SSE transect of the Red Sea. Oxygen concentrations are given in µmol kg^{-1}. The depth positions of sediment cores GeoTü KL11 and GeoB 5844-2 are indicated. The blue stippled line represents the base of the pycnocline (Cember, 1988).

The paleoceanography of the Red Sea during the Late Quaternary was closely linked to global sea-level changes regulating the exchange of water masses between the Red Sea and the Indian Ocean. Reduced water exchange occurred during glacial sea-level lowstands, leading to a drastic increase in Red Sea SSS (Thunell et al., 1988; Locke and Thunell, 1988). The glacial salinity increase resulted in a decrease in the abundance of pteropods and planktic foraminifera (Almogi-Labin et al., 1998), and ultimately led to the development of "aplanktic" zones, when the upper salinity limits for planktic foraminifera were exceeded (Fenton et al., 2000; Trommer et al., 2011). The strong salinity changes are reflected by high-amplitude fluctuations of the planktic $\delta^{18}O$, with glacial-to-interglacial differences of up to ~5 ‰ (Hemleben et al., 1996). The planktic $\delta^{18}O$ record facilitated the reconstruction of detailed eustatic sea-level fluctuations for the past 500 kyr, allowing for the evaluation of glacial lowstands and interglacial highstands, short-term fluctuations in response to abrupt climate change, and polar ice sheet dynamics (Rohling et al., 1998, 2004, 2009; Siddall et al., 2003; Arz et al., 2007; Bouilloux et al., 2013; Grant et al., 2014).

The glacial-interglacial changes in SSS and alternating exposure and flooding of shallow shelf areas in the Gulfs of Aqaba and Suez modulated the formation rate of intermediate and deep-water masses in the northern Red Sea, and thus the ROC. Despite strongly increased SSS during glacials (Hemleben et al., 1996), the abolition of dense water formation sites at low sea levels

resulted in a reduction of the ROC as indicated by increased proportions of low-oxygen-tolerant taxa and drops in the diversity of deep-sea benthic foraminifera (Badawi et al., 2005). The available benthic stable isotope records, which could provide further insights into deep-water circulation changes, are either intermittent (Hemleben et al., 1996) or combine epi- and infaunal taxa (Arz et al., 2007), which involves potential biases concerning the influence of strong porewater and metabolic

90   effects (Theodor et al., 2016). To date, a detailed reconstruction of changes in deep-water circulation and ventilation is still missing. Particularly, it remains unclear how the glacial ROC is influenced by the millennial-scale climate variability of the North Atlantic and if the stable carbon isotopic composition of the dissolved inorganic carbon (DIC) of the deep-water mass is also influenced by the African-Indian monsoon system.

95   These open questions will be addressed with our study. Especially, we present the first high-resolution composite epibenthic foraminiferal stable isotope record of Marine Isotope Stage (MIS) 3 from intermediate water depth of the central Red Sea. The data are evaluated for (i) orbital and millennial-scale variability, and (ii) relations between the regional hydrological and biogeochemical processes with the climate variability of the high and low latitudes.

2 Material and Methods

100   Sediment core GeoTü KL11 (in the following referred to as KL11; Figs. 1, 3) was recovered in 1987 during RV *Meteor* cruise M5/2 (Hemleben, 1996). It was retrieved from the central Red Sea (18°44.5' N and 39°20.6' E) at 825 m water depth. Total core recovery was 21.0 m. For this study, we sampled the interval from 194 to 391 cm at 1 to 2 cm spacing, summing up to a total of 104 samples. We wet sieved 2–3 g freeze-dried sediment of each sample over a 63 µm mesh. The residue was dried at 38 °C and subsequently dry sieved over a 125 µm mesh. The fraction >125 µm was investigated in our study.

105   For stable isotope analyses, we selected the benthic foraminiferal species *Cibicides mabahethi*, *Discorbinella bertheloti* s.l., and *Hanzawaia boueana* s.l., all inhabiting a preferentially epifaunal microhabitat (Rathburn and Corliss, 1994; Edelman-Furstenberg et al., 2001; Murray, 2006; Margreth et al., 2009). The species were not present in all samples, but exhibited concurrent occurrences in some intervals, allowing for the generation of a composite stable isotope record with an average of the up to three epibenthic isotope measurements. For each species, at least 5 individuals were selected per sample, and their

110   diameters and preservation states were documented. The stable isotope analyses were performed on a Finnigan MAT 253 mass spectrometer in conjunction with an automatic Kiel IV carbonate preparation device at the Leibniz-Laboratory for Radiometric Dating and Stable Isotope Research, Kiel. Sample reaction was induced by individual acid addition (99 % H_3PO_4 at 75 °C) under vacuum. The evolved carbon dioxide was analysed eight times for each sample. As documented by the performance of international [NBS19: +1.95‰ VPDB (^{13}C), -2.20 ‰ VPDB (^{18}O); IAEA-603: +2.46 ‰ VPDB (^{13}C), -2.37 ‰ VPDB (^{18}O)]

115   and laboratory-internal carbonate standards [Hela: +0.91 ‰ VPDB (^{13}C), +2.48 ‰ VPDB (^{18}O); HB1: -12.10 ‰ VPDB (^{13}C), -18.10 ‰ VPDB (^{18}O); SHK: +1.74 ‰ VPDB (^{13}C), -4.85 ‰ VPDB (^{18}O)], analytical precision of stable isotope analysis is better than ±0.08 ‰ for δ^{18}O and ±0.05 ‰ for δ^{13}C. Values are given in δ notation versus VPDB.

120 Various age models have been published for core KL11, mainly based on graphical correlations of the planktic δ¹⁸O record with the global standard δ¹⁸O record (Hemleben et al., 1996), the Antarctic ice core record (Siddall et al., 2003), the Soreq speleothem record (Grant et al., 2012), and further refinement of the latter by including AMS¹⁴C ages (Hartman et al., 2020). The consideration of AMS¹⁴C ages in the Red Sea may be problematic because of uncertainties in reservoir ages and potential early diagenetic effects (Rohling et al., 2008). Nevertheless, in order to avoid the tuning of our record to external time series,

125 we established our age model for MIS 3 of KL11 by including two AMS¹⁴C dates (Schmelzer, 1998), and correlating the composite epibenthic δ¹⁸O record with the benthic δ¹⁸O record of the well-dated core GeoB 5844-2 from 963 m water depth of the northernmost Red Sea (Arz et al., 2007) (Figs. 1, 4, Table 1). The age model of the interval 25-65 ka B.P. of GeoB5844-2 is based on 5 AMS¹⁴C dates, and on correlation of the magnetic paleointensity record to the North Atlantic paleointensity stack in the interval older than 40 kyr (Fig. 4). For consistency with the published radiocarbon ages and age model of Arz et

130 al. (2007), we refrained from re-calibration of the AMS¹⁴C dates using newer calibration curves. The synchronization of the two cores is justified, because their benthic δ¹⁸O records resemble each other due to the common main deep-water source situated in the northern Red Sea. The deep-water mass is relatively homogenous, with similar temperatures and salinities across the basin (Cember, 1988; Woelk and Quadfasel, 1996). A similar homogeneity of deep-water temperature and salinity obviously persisted also during the past glacial, illustrated by the close resemblance of the benthic δ¹⁸O records from the

135 northern and central Red Sea (Fig. 4). According to our age model, the studied core section covers the time interval from 62.1 to 28.4 ka B.P., with an average sample resolution of 330 ± 90 years.
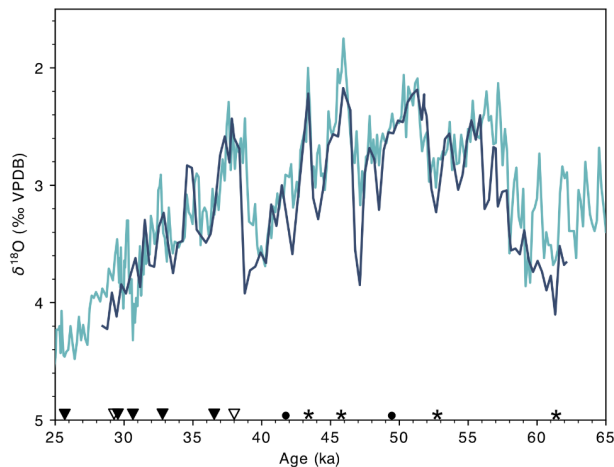
Figure 4. Alignment of benthic $\delta^{18}O$ records of cores KL11 from the central Red Sea (dark blue) and GeoB5844-2 from the northern Red Sea (light blue). Black triangles represent the radiocarbon dates, and black dots the paleomagnetic data used for the establishment of the age model of GeoB5844-2 (Arz et al., 2007). The age model of KL11 is based on two radiocarbon dates of KL11 (white triangles; Schmelzer, 1998) and the graphical correlation of the $\delta^{18}O$ records. Black asterisks represent the graphical tie-points.

Table 1 Data used for establishing the age model for the studied section of KL11.

Core depth (cm)	Age (cal. ka B.P.)	Datum	Reference
199.5	29.29 ± 0.35	AMS^{14}C, KL11	Schmelzer (1998)
250.5	38.00 ± 0.71	AMS^{14}C, KL11	Schmelzer (1998)
278.5	43.38	$\delta^{18}O$ of GeoB5844-2	Arz et al. (2007)
292.5	45.92	$\delta^{18}O$ of GeoB5844-2	Arz et al. (2007)
331.5	52.67	$\delta^{18}O$ of GeoB5844-2	Arz et al. (2007)
385.5	61.32	$\delta^{18}O$ of GeoB5844-2	Arz et al. (2007)

3 Results

The stable isotope values exhibit specific offsets between the different taxa in both $\delta^{18}O$ and $\delta^{13}C$. The calculation of average offsets between the species is based on 60 paired analyses of *C. mabahethi* and *D. bertheloti* s.l. and 40 paired analyses of *C. mabahethi* and *H. boueana* s.l.. Based on *C. mabahethi* as the reference value, the mean $\delta^{18}O$ deviation of *D. bertheloti* s.l. is -0.19 ± 0.30 ‰ and that of *H. boueana* s.l. is +0.02 ± 0.24 ‰. The corresponding mean $\delta^{13}C$ deviations are -0.09 ± 0.30 ‰ for *D. bertheloti* s.l. and +0.17 ± 0.19 ‰ for *H. boueana* s.l. (Fig. 5). The mean $\Delta\delta^{18}O$ and $\Delta\delta^{13}C$ values were used to adjust the stable isotope values of *D. bertheloti* s.l. and *H. boueana* s.l. to that of *C. mabahethi* and to generate the composite stable isotope records, which are described and evaluated below. The average standard deviation for the composite $\delta^{18}O$ and $\delta^{13}C$ records is ±0.16 ‰ and ±0.13 ‰, respectively. These values are considerably lower when compared to the observed amplitudes of temporal fluctuations (Figs. 6-8).
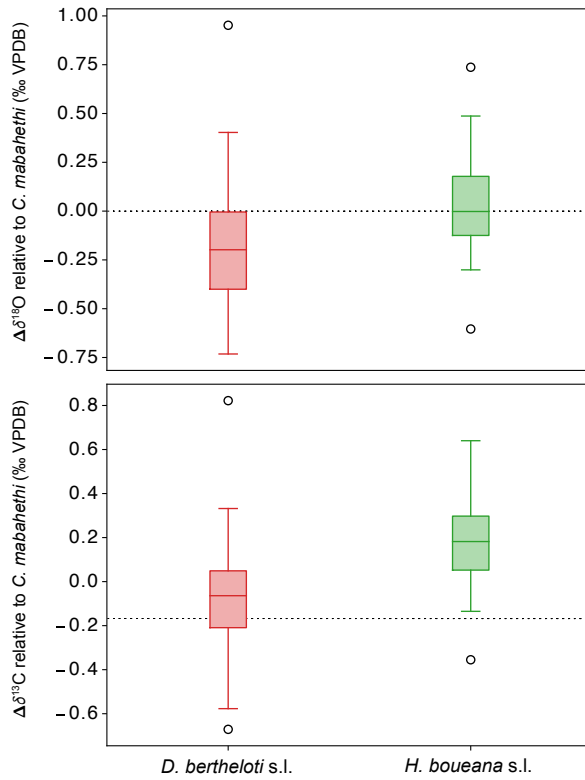
Figure 5. Box plots for the $\delta^{18}O$ and $\delta^{13}C$ deviations of *D. bertheloti* s.l. and *H. boueana* s.l. with reference to *C. mabahethi* in samples from MIS 3 of KL11.

160

The composite $\delta^{18}O$ record fluctuates between approximately 2.2 and 4.2 ‰ VPDB and shows rapid millennial-scale fluctuations, superimposed by a long-term trend from high to low values and back to high values. The short-term $\delta^{18}O$ fluctuations are in the order of 0.5 to 1.5 ‰. Pronounced maxima are centred around 61 ka, 47 ka, 39 ka, and 29 ka B.P. (Fig. 6a).

165
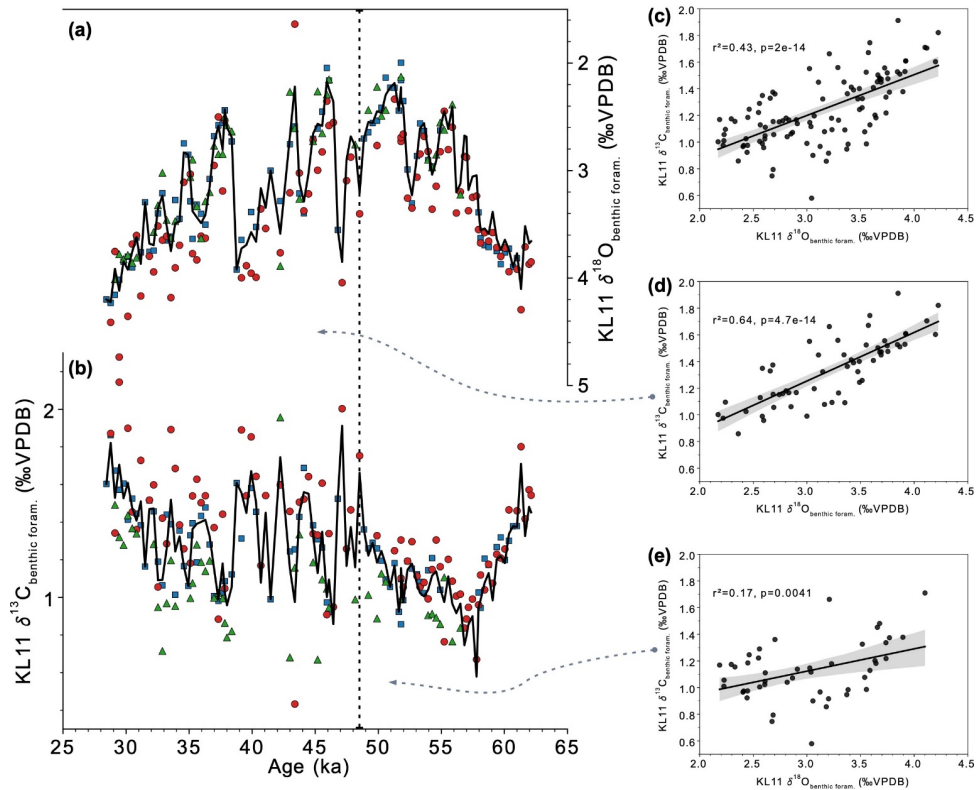
Figure 6. Composite stable **(a)** oxygen and **(b)** carbon isotope records for the interval ~62–28 ka B.P. of KL11 (black lines), representing the averages of up to three analysed benthic foraminiferal species. Before calculating the averages, the isotope values of *Discorbinella bertheloti* s.l. and *Hanzawaia boueana* s.l. were corrected by their mean species-specific offsets from the signal of *Cibicides mabahethi,* as shown in Fig. 5. The mean standard deviation of the calculated averages in the composites are ±0.16 ‰ for $\delta^{18}O$ and ±0.13 ‰ for $\delta^{13}C$. The markers indicate isotopic measurements of *C. mabahethi* (blue squares), *D. bertheloti* s.l. (red dots) and *H. boueana* s.l. (green triangles). The correlation between composite epibenthic $\delta^{18}O$ and $\delta^{13}C$ data are shown in **(c)** for the entire time interval, and separated for the intervals of **(d)** 48.5 to 28.4 ka B.P., and **(e)** 62.1 to 48.5 ka B.P.. The shaded area around the calibration indicates the 95% confidence interval of the regressions.

The values of the composite $\delta^{13}C$ record fluctuate between approximately 0.6 and 1.9 ‰ VPDB. The record is also characterized by millennial-scale fluctuations, which are, however, of lower amplitude (~0.5 to 1 ‰) when compared to those of the $\delta^{18}O$ record. In addition, the short-term changes of the $\delta^{13}C$ record are more pronounced in the interval between 48.5 and 28.4 ka B.P. while a more gradual $\delta^{13}C$ decrease is observed between 62.1 and 48.5 ka B.P. (Fig. 6b).

180

Accordingly, the $\delta^{18}O$ and $\delta^{13}C$ records reveal distinct differences in their correlation across the studied time interval. While the correlation of the entire composite isotope records delivers a coefficient of determination (R^2) of 0.43, it is considerably higher with $R^2 = 0.64$ for the interval 48.5–28.4 ka B.P. but only $R^2 = 0.17$ for the interval 62.1–48.5 ka B.P. (Fig. 6c, d and e).

185 **4 Discussion**

The epibenthic stable oxygen and carbon isotope records of KL11 display high-amplitude millennial-scale fluctuations (Fig. 6), suggesting rapid changes in deep-water temperature and/or salinity, and shifts in the deep-water residence time and organic matter fluxes of the central Red Sea. Despite potential uncertainties in the age model, the pattern in the epibenthic $\delta^{18}O$ record of KL11 closely resembles that of the high-latitude climate variability as documented in the Greenland NGRIP ice core record

190 (Figs. 7, 8) (NGRIP member, 2004; Svensson et al., 2008; Wolf et al., 2010). Specifically, low $\delta^{18}O$ values in KL11 coincide with Dansgaard-Oeschger interstadials and also exhibit the typical pattern of interstadial events, comprising a sharp and rapid increase phase, a plateau phase, and a slower decrease phase (e.g., 51, 46, 38 ka). High $\delta^{18}O$ values in KL11 coincide with stadials. Particularly high $\delta^{18}O$ values are related to Heinrich stadials (Figs. 7, 8). The close association of deep-water formation processes in the northern Red Sea and high northern latitude climate variability is nicely illustrated by the difference between

195 the epibenthic (deep-water) $\delta^{18}O$ record of KL11 and the planktic (surface-water in the vicinity of deep-water formation sites) $\delta^{18}O$ record of GeoB5844-2 (Fig. 7b). The $\Delta\delta^{18}O$ record reveals maximum values for stadials and Heinrich events, highlighting the formation of significantly colder and probably also more saline water masses at deep-water formation sites during northern hemisphere cold events. This provides evidence for a dominant northern hemisphere climate control of Red Sea deep-water formation and, thus, on the ROC during MIS 3. This interpretation is generally corroborated by the close resemblance to the

200 $\Delta\delta^{18}O$ record based on the endobenthic (*Bulimina marginata*) and planktic (*Globigerinoides ruber*) $\delta^{18}O$ data of GeoB5844-2 (7c). However, the consideration of *B. marginata* is less reliable since this species prefers an endobenthic microhabitat (Jorissen and Wittling, 1999), and, therefore, its $\delta^{18}O$ signal may additionally reflect changes in the alkalinity gradient of the porewater (Schmiedl and Mackensen, 2006).

Figure 7. Comparison of epibenthic and planktic stable oxygen isotope records from the Red Sea, their resulting difference, and the Greenland stable oxygen isotope record. **(a)** $\delta^{18}O$ record of the North Greenland Ice Core Project (NGRIP members, 2004) against the extended GICC05 age scale (Svensson et al., 2008; Wolf et al., 2010). **(b)** Difference in the stable oxygen isotope records ($\Delta\delta^{18}O$) of the composite epibenthic $\delta^{18}O$ of KL11 from the central Red Sea and the planktic (*Globigerinoides ruber*) $\delta^{18}O$ of GeoB5844-2 from the northern Red Sea (Arz et al., 2007). For calculation of the $\Delta\delta^{18}O$ values, the single records were resampled at a spacing of 330 years. **(c)** Difference in the stable oxygen isotope records ($\Delta\delta^{18}O$) of the endobenthic (*Bulimina marginata*) and planktic (*G. ruber*) $\delta^{18}O$ of GeoB5844-2 from the northern Red Sea (Arz et al., 2007). **(d)** Planktic (*G. ruber*) $\delta^{18}O$ of GeoB5844-2 from the northern Red Sea (Arz et al., 2007). **(e)** Composite epibenthic $\delta^{18}O$ of KL11 from the central Red Sea (blue) and endobenthic (*B. marginata*) $\delta^{18}O$ of GeoB5844-2 from the northern Red Sea (stippled orange; Arz et al., 2007). The horizontal stippled lines in the $\Delta\delta^{18}O$ records mark the mean values. Grey bars represent northern hemisphere stadials and Heinrich events.
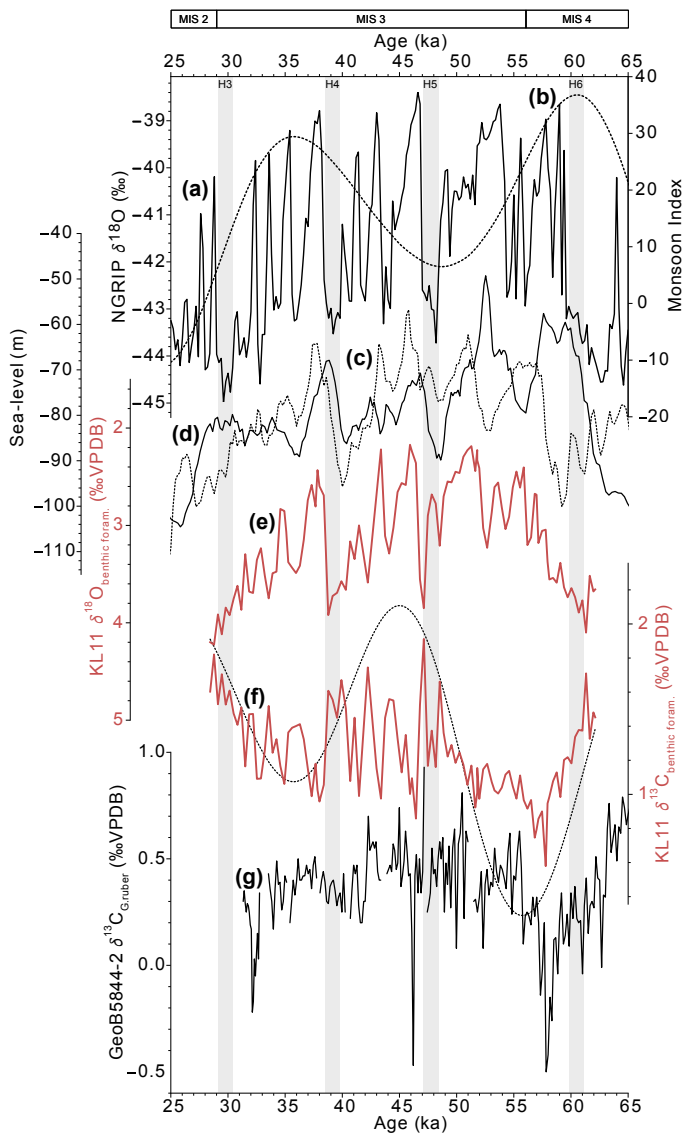
Figure 8. Composite epibenthic stable oxygen and carbon isotope records of the central Red Sea compared with the planktic stable carbon isotope record of the northern Red Sea, sea-level reconstructions for the Red Sea, and climate changes of the high northern latitudes for marine isotope stages (MIS) 2 to 4. **(a)** δ^{18}O record of the North Greenland Ice Core Project (NGRIP members, 2004) against the extended GICC05 age scale (Svensson et al., 2008; Wolf et al., 2010). **(b)** Monsoon index calculated according to Rossignol-Strick (1983), based on the June 21 insolation at 23.45° N and at the equator (Laskar et al., 2004). **(c)** Sea-level reconstructions for the northern Red Sea (dashed line, Arz et al., 2007) and **(d)** central Red Sea (black line, Siddall et al., 2003; Rohling et al., 2008). **(e)** Composite epibenthic δ^{18}O record of KL11 from the central Red Sea. **(f)** Composite epibenthic δ^{13}C record of KL11 from the central Red Sea. The stippled line represents the band pass filtered precession (23 kyr) component of the epibenthic δ^{13}C record. Note that minima in the δ^{13}C precession component correspond to maxima in the monsoon index. **(g)** δ^{13}C record of the planktic foraminifer *Globigerinoides ruber* white of GeoB 5844-2 from the northern Red Sea (Arz et al., 2007). Note that the insolation maximum centered around 58–62 ka B.P. is associated with a transient decrease of planktic and epibenthic δ^{13}C values. The positions of Heinrich stadials H3–H6 are indicated by light grey bars.

Heinrich stadials are associated with a strong reduction or even cessation of North Atlantic Deep-Water formation (McManus et al., 2004; Denton et al., 2010). Proxy data and model results demonstrated that the slow-down of the Atlantic Meridional Overturning Circulation also influenced the hydrology of mid- to low-latitude regions in the northern hemisphere, leading to megadroughts in northern Africa and the Mediterranean region (Mulitza et al., 2008; Hamann et al., 2008; Ehrmann et al., 2017; Allard et al., 2021), and weakening of the Indian summer monsoon (Schulz et al., 1998). It is likely that during these droughts, enhanced evaporation also resulted in increased sea-surface salinity in the northern Red Sea, fostering the formation of dense waters in this region. Previous studies have confirmed a strong influence of changes in the Mediterranean and North Atlantic climate on the environmental changes in the northern Red Sea (Arz et al., 2003a, b, 2007; Lamy et al., 2006). Alkenone temperature reconstructions for the northern Red Sea display a general cooling trend during MIS 3, punctuated by short-term sea-surface temperature (SST) drops in the order of 1 to 4 °C during Heinrich stadials. We speculate that the strong cooling could be associated with the inflow of cold air masses from the north responding to phases of intensified Siberian High. The strength of the Siberian High is linked to the North Atlantic climate variability. It is generally stronger during glacials due to enhanced surface cooling of the Eurasian continent (Vandenberghe et al., 2006). In the eastern Mediterranean region, northeasterly outbreaks of cold air are linked to the strength of the Siberian High (Rohling et al., 2002; Casford et al., 2003). The close correspondence of grain-size in Asian loess deposits and the Greenland ice core record suggest a stronger Siberian High during stadials of the last glacial period (Vandenberghe et al., 2006; Cheng et al., 2022), possibly also explaining the strong SST drops in the northern Red Sea during Heinrich events. Pollen data from the Aegean region suggest extremely severe climate deterioration during Heinrich stadial H5 (Müller et al., 2011), which is also reflected in the deep-sea δ^{18}O record of the Red Sea (Figs. 6-8).

Similarly, the reconstructed sea-level fluctuations in the northern Red Sea occurred also in phase with northern hemisphere climate variability, with transient sea-level rises of up to 25 m during Greenland interstadials (Arz et al., 2007). These results contrast with earlier findings from the central Red Sea, where estimated short-term sea-level changes are in the order of 35 m and occurred in phase with Antarctic climate changes (Siddall et al., 2003) suggesting a strong southern meltwater component. Subsequent model simulations and comparison with stable oxygen isotope data suggest similar meltwater contributions from both Antarctic and northern ice sheets during the last glacial period (Rohling et al., 2004) (Fig. 8d). To date, the establishment of accurately dated sea-level records is limited by the various age scales used in Greenland and Antarctic ice core records (review in Siddall et al. 2008). Some of the discrepancies in the available sea-level reconstructions from the Red Sea may be attributed to the different age model strategies, involving potential dating uncertainties and diagenetic biases (Rohling et al., 2008). In addition, the extraction of the sea-level component from the benthic $\delta^{18}O$ signal strongly depends on the correct reconstruction of temperature and salinity effects at deep-water formation sites, which appears challenging. Despite these biases and conflicting reconstructions millennial-scale sea-level changes during the last glacial period seem to essentially follow an Antarctic climate pattern (Siddall et al. 2008). However, the subsequent study of Grant et al. (2012) from the eastern Mediterranean Sea suggested that the large-scale sea-level variability reflects a global signature of climate changes recorded in both Antarctic and Greenland ice cores.

The close resemblance of the epibenthic $\delta^{18}O$ record with that of the Greenland ice core record suggest a direct atmospheric control on short-term changes in deep-water circulation during the last glacial period. Since maximum deep-water formation is observed during Heinrich stadials, when sea-level dropped, the moderate further exposure of shelf areas in the northern Red Sea obviously did not play a dominant role on deep-water formation. Instead, the more restricted exchange between the Red Sea and the Indian Ocean and the associated SSS rise in the Red Sea likely facilitated dense-water formation (Arz et al., 2007) (Figs. 7, 8). However, the succession of Dansgaard-Oeschger and Heinrich events is largely overprinted by salinity effects in the planktic $\delta^{18}O$ records of the Red Sea (Siddall et al., 2003; Arz et al., 2007) (Fig. 7). According to these findings, cooling and enhanced evaporation rates prevailed in the northern Red Sea region during Heinrich stadials and fostered the formation of dense waters in the deep-water formation sites. In the time interval ~49–28 ka B.P., epibenthic $\delta^{18}O$ and $\delta^{13}C$ records of KL11 show a positive correlation, with high $\delta^{18}O$ values during Heinrich stadials being associated with high epibenthic $\delta^{13}C$ values. The lack of differences between the $\delta^{13}C$ records of KL11 and GeoB5844-2 affirm that the epibenthic stable carbon isotope can be used to reflect the residence time. This confirms our conclusion of more vigorous ventilation of deep-water masses with low residence times during Heinrich stadials and reduced ventilation with the presence of older and thus ^{12}C-enriched deep-water masses during Dansgaard-Oeschger interstadials.

For the correct interpretation of the deep-sea $\delta^{13}C$ record, the potential contribution of $\delta^{13}C$ changes of dissolved inorganic carbon (DIC) in the source areas of deep-water formation in the northern Red Sea must be considered. Therefore, we compared

the epibenthic δ^{13}C record of KL11 with the δ^{13}C record of the planktic foraminifer *Globigerinoides ruber* white of GeoB 5844-2 from the northernmost Red Sea (Arz et al., 2007) (Fig. 8). The epibenthic carbon isotopic composition reflects the addition of ^{12}C to the intermediate and deep water through decomposition of sinking organic matter. Despite the preferentially epifaunal lifestyle of the measured taxa, additional porewater effects of around 0.2–0.5 ‰ cannot be ruled out as suggested from analyses on morphologically similar species of the genera *Cibicides* and *Cibicidoides* (McCorkle et al., 1990; Schmiedl et al., 2004; Theodor et al., 2016). Various studies have shown that the δ^{13}C of *G. ruber* reflects not only the δ^{13}C of ambient DIC, but is also influenced by biological fractionation effects, mainly by algal photosymbiosis and the metabolism of the foraminifer (Rohling and Cooke, 1999; Schiebel and Hemleben, 2017, and references therein). Accordingly, the δ^{13}C of *G. ruber* commonly deviates significantly from δ^{13}C$_{DIC}$. Depending on the magnitude of the different effects, the deviations of δ^{13}C$_{G.ruber}$ from δ^{13}C$_{DIC}$ range from +1 ‰ due to symbiotic enrichment (Bemis et al., 1998), to -0.5 to -1 ‰ due to metabolic depletion (Niebler, 1995; Katz et al., 2010; Birch et al., 2013). Despite these offsets, the epibenthic and planktic δ^{13}C records of KL11 reflect a generally similar long-term trend, particularly in the older part of the record. However, the planktic δ^{13}C record lacks systematic Heinrich-stadials-associated fluctuations. Thus, the alteration of surface water δ^{13}C$_{DIC}$ by millennial-scale changes in productivity and addition of ^{12}C from land can be largely ruled out. These processes play a more prominent role on orbital time scales. Specifically, last glacial δ^{13}C values of the Red Sea surface waters are approximately 0.5–1.0 ‰ lower than Holocene values (Schmelzer, 1998; Bouilloux et al., 2013), suggesting the redistribution of carbon from exposed shelf areas into the Red Sea basin during glacial sea-level low-stands.

The decoupling of the δ^{18}O and δ^{13}C records in the interval ~62–49 ka B.P. suggests the additional influence of orbital-scale regional biogeochemical processes on the δ^{13}C signal in the central Red Sea (Fig. 8). The core position of KL11 is situated close to the border between the more oligotrophic central and northern Red Sea and the mesotrophic to eutrophic area in the southern Red Sea (Raitsos et al., 2013). According to the modern situation, changes in surface-water productivity at site KL11 depend on vertical mixing and formation of eddies during winter (Eshel and Naik, 1997; Raitsos et al., 2013) but may also be influenced by the intrusion of nutrient-rich intermediate waters from the Gulf of Aden during summer (Trommer et al., 2010; Dreano et al., 2016).

The past exchange of water masses between the Red Sea and Indian Ocean and the advection of nutrient-rich waters from the Gulf of Aden through the strait of Bab al-Mandab depend on orbital and suborbital glacio-eustatic changes, and shifts in monsoon wind intensity (Siddall et al., 2004; Trommer et al., 2011; Bouilloux et al., 2013). During the time interval ~60–50 ka B.P., the global sea-level was approximately 60 m lower than at present, but higher than during the sea-level low stands of MIS 4 (approximately -100 m) and the last glacial maximum (approximately -120 m) (Siddall et al., 2003; Rohling et al., 2004; Grant et al., 2014) (Fig. 8). Within MIS 2-4, sea-level was at a maximum between ~60 and 50 ka B.P.. Accordingly, the

340   exchange of intermediate waters likely persisted during this period, including the inflow of nutrient-rich GAIW during summer, particularly during phases of enhanced summer monsoon winds (Fig. 8).

       The time interval 58–62 ka B.P. coincides with the stronger of two maxima in the northern hemisphere monsoon index during MIS 3 (Fig. 8b). The monsoon index has been calculated according to Rossignol-Strick (1983), based on the June 21 insolation
345   gradient between 23.45° N and at the equator (Laskar et al., 2004). Generally, maxima in African-Asian summer monsoon are coherent with insolation maxima (Cheng et al., 2016). However, upwelling proxies from marine sediment cores of the Arabian Sea exhibit time lags of ~8 kyr between insolation and monsoon maxima, which has been attributed to the impact of ice volume of the Northern Hemisphere and the transport of latent heat from the southern subtropical Indian Ocean to the Tibetan Plateau (Clemens and Prell, 2003; Clemens et al., 2010). A new model study demonstrated that the observed time lag in the Arabian
350   Sea did not necessarily document changes in Indian summer monsoon intensity. It may rather be caused by shifts of the upwelling area from coastal regions during insolation maxima to more open-ocean areas during insolation minima (Jalihal et al., 2022). The decrease of epibenthic δ^{13}C in KL11 lags the monsoon index maximum by only ~3.5 kyr which is comparable to the observed lags of Mediterranean sapropels (Lourens et al., 1996), and also lags in Asian speleothem records (Clemens et al., 2010). The close relation of the monsoon index and epibenthic δ^{13}C suggests a more or less immediate response of surface-
355   water productivity and related organic matter fluxes at site KL11 to the strength of the summer monsoon. Our results support previous evidence from planktic foraminifera, which exhibit a close correspondence between the high-productivity indicator *Globigerinita glutinata* and summer insolation at site KL11 during the last interglacial period (Trommer et al., 2011). The development of summer phytoplankton blooms in the southern part of the modern Red Sea is related to the intrusion of nutrient-rich intermediate waters from the Gulf of Aden, which can be traced as far north as 19° N (Trommer et al., 2010; Dreano et
360   al., 2016). The different proxy data suggest that this process was intensified in the past during phases of increased Indian summer monsoon, and that nutrient-rich waters reached the position of KL11 temporarily during MIS 3. The timing suggests that the nutrient-rich waters were derived from areas along the southern Arabian Peninsula where maximum upwelling occurred during phases of intensified Indian summer monsoon (Jalihal et al., 2022).

5 Conclusions

365   We established a high-resolution composite epibenthic stable oxygen and carbon isotope record from the central Red Sea for the last glacial period. The records show high-amplitude variations during MIS 3, suggesting millennial-scale changes in the thermohaline circulation of the Red Sea. Despite generally reduced ROC during glacial sea-level lowstands, deep-water formation increased during cold and hyper-arid conditions in the northern Red Sea borderlands. Inversely, the formation of dense waters was reduced during warmer and more humid conditions resulting in a diminished ROC.

370

The millennial-scale changes in aridity in the northern Red Sea region are in phase with the abrupt climate variability of the high northern latitudes as documented in the Greenland ice core record which could suggest a link to the strength of the Siberian High and related inflow of cold air masses to the sites of Red Sea deep-water formation. Our results suggest that the regional

375 hydroclimatic changes modulate the thermohaline circulation of the Red Sea during glacial boundary conditions. Instead, millennial-scale sea-level changes and related changes in the exchange between the Red Sea and the Indian Ocean play a subordinate role in the preconditioning of dense water formation in the northern Red Sea. This is also shown by the lack of coherent millennial-scale changes in the planktic stable isotope records from the northernmost Red Sea representing the general source signal in the area of deep-water formation.

380

The KL11 stable oxygen and carbon isotope records are decoupled in the early part of MIS 3, caused by a transient decrease of δ^{13}C values in phase with an increase of northern hemisphere summer insolation around 55–60 ka B.P.. This suggests a connection between the biogeochemical processes of the central Red Sea to the African-Indian monsoon dynamics. During the summer monsoon maximum and concomitant moderate sea-level rise, nutrient-rich intermediate waters intruded from the Gulf

385 of Aden and delivered nutrients as far north as 19° N. The influx of nutrients fuelled surface-water productivity at site KL11 in the central Red Sea. The associated remineralization of sinking organic matter led to the observed transient decrease in epibenthic δ^{13}C values.

Data availability

The new data are available in the supplement of this paper.

390 **Author contributions**

GS and WE initiated the initial project (REVENT). RHH was in charge of the sample processing and species selection. NA performed the stable isotope analysis. RHH and GS wrote the first draft of the paper. HWA contributed planktic isotope data. All authors contributed to the interpretation and discussion of the data, and to the writing of the submitted paper.

Competing interests

395 The authors declare that they have no conflict of interest.

Acknowledgments

We acknowledge the efforts of the master and crew of "RV *Meteor*", the chief scientist Hjalmar Thiel (Hamburg) and the group leader Christoph Hemleben (Tübingen) for their efforts during cruise M5/2 in 1987. We are grateful to Constantin Mey

and Manja Oldhaver for technical assistance in the laboratory. We thank the reviewers for thoughtful and constructive reviews and the editor for smooth handling of the manuscript. Funded by the Deutsche Forschungsgemeinschaft (DFG, German Research Foundation) under projects Schm 1180/26-1, Eh 89/23-1, and Germany's Excellence Strategy – EXC 2037 'CLICCS - Climate, Climatic Change, and Society' – Project Number: 390683824. The study is a contribution to the Center for Earth System Research and Sustainability (CEN) of Universität Hamburg.

References

Allard J. L., Hughes, P. D., and Woodward, J. C.: Heinrich Stadial aridity forced Mediterranean-wide glacier retreat in the last cold stage, Nat. Geosci., 14, 197–205, https://doi.org/10.1038/s41561-021-00703-6, 2021.

Almogi-Labin, A., Hemleben, C., and Meischner, D.: Carbonate preservation and climatic changes in the central Red Sea during the last 380 kyr as recorded by pteropods, Mar. Micropaleontol., 33, 87–107, https://doi.org/10.1016/S0377-8398(97)00034-0, 1998.

Arz, H. W., Pätzold, J., Müller, P. J., and Moammar, M.O.: Influence of Northern Hemisphere climate and global sea level rise on the restricted Red Sea marine environment during termination I, Paleoceanography, 18, 1053, https://doi.org/10.1029/2002pa000864, 2003a.

Arz, H. W., Lamy, F., Pätzold, J., Müller, P. J., and Prins, M.: Mediterranean Moisture Source for an Early-Holocene Humid Period in the Northern Red Sea, Science, 300, 118–121, https://doi.org/10.1126/science.1080325, 2003b.

Arz, H. W., Lamy, F., Ganopolski, A., Nowaczyk, N., and Pätzold, J.: Dominant Northern Hemisphere climate control over millennial-scale glacial sea-level variability, Quat. Sci. Rev., 26, 312–321, https://doi.org/10.1016/j.quascirev.2006.07.016, 2007.

Badawi, A., Schmiedl, G., and Hemleben, C.: Impact of late Quaternary environmental changes on deep-sea benthic foraminiferal faunas of the Red Sea, Mar. Micropaleontol., 58, 13–30, https://doi.org/10.1016/j.marmicro.2005.08.002, 2005.

Bemis, B. E. and Spero, H. J.: Reevaluation of the oxygen isotopic composition of planktonic foraminifera: Experimental results and revised paleotemperature equations, Paleoceanography, 13, 150–160, https://doi.org/10.1029/98PA00070, 1998.

Birch, H., Coxall, H. K., Pearson, P. N., Kroon, D., and O'Regan, M.: Planktonic foraminifera stable isotopes and water column structure: Disentangling ecological signals, Mar. Micropaleontol., 101, 127–145, https://doi.org/10.1016/j.marmicro.2013.02.002, 2013.

Bouilloux, A., Valet, J.-P., Bassinot, F., Joron, J.-L., Dewilde, F., Blanc-Valleron, M.-M., and Moreno, E.: Influence of seawater exchanges across the Bab-el-Mandeb Strait on sedimentation in the Southern Red Sea during the last 60 ka, Paleoceanography, 28, 675–687, https://doi.org/10.1002/2013PA002544, 2013.

Casford, J.S.L., Rohling, E.J., Abu-Zied, R.H., Jorissen, F.J., Leng, M., Schmiedl, G., Thomson, J.: A dynamic concept for
435   eastern Mediterranean circulation and oxygenation during sapropel formation. Palaeogeogr., Palaeoclimatol., Palaeoecol.,
190, 103-119, https://doi.org/10.1016/S0031-0182(02)00601-6, 2003.

Cember, R. P.: On the sources, formation, and circulation of Red Sea deep water, J. Geophys. Res., 93, 8175–8191,
https://doi.org/10.1029/JC093iC07p08175, 1988.

Cheng, H., Edwards, L., Sinha, A., Spötl, C., Yi, L., Chen, S., Kelly, M., Kathayat, G., Wang, X., Li, X., Kong, X., Wang, Y.,
440   Ning, Y., and Zhang, H.: The Asian monsoon over the past 640,000 years and ice age terminations, Nature, 534, 640–646,
https://doi.org/10.1038/nature18591, 2016.

Cheng, L., Song, Y., Yang, L., Chang, H., Wu, Y., Long, H., Miao, X., Dong, Z.: Variations of the intensity of the Siberian
High during the last glacial revealed by the sorting coefficient of loess-paleosol deposits in Eastern Central Asia.
Paleoceanogr. Paleoclimatol., 37, e2022PA004468, https://doi.org/10.1029/2022PA004468, 2022.

445   Clemens, S. C., and Prell, W. L.: A 350,000 year summer-monsoon multi-proxy stack from the Owen Ridge, Northern Arabian
Sea. Mar. Geol., 201, 35–51, https://doi.org/10.1016/S0025-3227(03)00207-X, 2003.

Clemens, S. C., Prell, W. L., and Sun, Y.: Orbital-scale timing and mechanisms driving Late Pleistocene Indo-Asian summer
monsoons: Reinterpreting cave speleothem δ^{18}O, Paleoceanography, 25, PA4207, https://doi.org/10.1029/2010PA001926,
2010.

450   Denton, G. H., Anderson, R. F., Toggweiler, J. R., Edwards, R. L., Schaefer, J. M., and Putnam, A. E.: The last glacial
termination, Science, 328: 1652–1656, https://doi.org/10.1126/science.1184119, 2010.

Dreano, D., Raitsos, D. E., Gittings, J., Krokos, G., Hoteit, I.: The Gulf of Aden Intermediate Water Intrusion Regulates the
Southern Red Sea Summer Phytoplankton Blooms, PloS ONE, 12, e0168440,
https://doi.org/10.1371/journal.pone.0168440, 2016.

455   Edelman-Furstenberg, Y., Scherbacher, M., Hemleben, C., and Almogi-Labin, A.: Deep-sea benthic foraminifera from the
Central Red Sea, J. Foram. Res., 48–59, https://doi.org/10.2113/0310048, 2001.

Ehrmann, W., Schmiedl, G., Beuscher, S., and Krüger, S.: Intensity of African Humid Periods estimated from Saharan dust
fluxes, PLoS ONE, 12, e0170989, https://doi.org/10.1371/journal.pone.0170989, 2017.

Eshel, G., and Naik, N. H.: Climatological coastal jet collision, intermediate water formation, and general circulation of the
460   Red Sea, J. Phys. Oceanogr., 27, 1233–1257, https://doi.org/10.1175/1520-0485(1997)027<1233:CCJCIW>2.0.CO;2,
1997.

Eshel, G., Cane, M. A., and Blumenthal, M. B.: Modes of subsurface, intermediate and deep water renewal in the Red Sea, J.
Geophys. Res., 99, 15941–15952, https://doi.org/10.1029/94JC01131, 1994.

Fenton, M., Geiselhart, S., Rohling, E. J., and Hemleben, C.: Aplanktonic zones in the Red Sea, Mar. Micropaleontol., 40,
465   277–294, https://doi.org/10.1016/S0377-8398(00)00042-6, 2000.

Grant, K. M., Rohling, E. J., Bar-Matthews, M., Ayalon, A., Medina-Elizalde, M., Ramsey, C. B., Satow, C., and Roberts, A. P.: Rapid coupling between ice volume and polar temperature over the past 150,000 years, Nature, 491, 744–747, https://doi.org/10.1038/nature11593, 2012.

Grant, K. M., Rohling, E. J., Ramsey, C. B., Cheng, H., Edwards, R. L., Florindo, F., Heslop, D., Marra, F., Roberts, A. P., Tamisiea, M. E., and Williams, F.: Sea-level variability over five glacial cycles, Nat. Commun., 5, 5076, https://doi.org/10.1038/ncomms6076, 2014.

Hamann, Y., Ehrmann, W., Schmiedl, G., Krüger, S., Stuut, J.-B., and Kuhnt, T.: Sedimentation processes in the eastern Mediterranean Sea during the Late Glacial and Holocene revealed by end-member modelling, Mar. Geol., 248, 97–114, https://doi.org/10.1016/j.margeo.2007.10.009, 2008.

Hartman, A., Torfstein, A., and Almogi-Labin, A.: Climate swings in the northern Red Sea over the last 150,000 years from εNd and Mg/Ca of marine sediments, Quat. Sci. Rev., 231, 106205, https://doi.org/10.1016/j.quascirev.2020.106205, 2020.

Hemleben, C.: Foraminiferal assemblages and sediments. In: Nellen, W., Bettac, W., Roether, W., Schnack, D., Thiel, H., Weikert, H., and Zeitzschel, B. (Eds.), MINDIK, Reise Nr. 5, 02. Januar 1987 – 24. September 1987 Band I. Meteor-Berichte, 96–1, 119–124, 1996.

Hemleben, C., Meischner, D., Zahn, R., Almogi-Labin, A., Erlenkeuser, H., and Hiller, B.: Three hundred eighty thousand year long stable isotope and faunal records from the Red Sea: Influence of global sea level change on hydrography, Paleoceanography, 11, 147–156, https://doi.org/10.1029/95PA03838, 1996.

Jalihal, C., Srinivasan, J., and Chakraborty, A.: Response of the low-level jet to precession and its implications for proxies of the Indian Monsoon, Geophys. Res. Lett., 49, e2021GL094760, https://doi.org/10.1029/2021GL094760, 2022.

Jorissen, F.J., and Wittling, I.: Ecological evidence from live-dead comparisons of benthic foraminiferal faunas off Cape Blanc (Northwest Africa). Palaeogeogr., Palaeoclimatol., Palaeoecol., 149, 151-170, https://doi.org/10.1016/S0031-0182(98)00198-9, 1999.

Katz, M. E., Cramer, B. S., Franzese, A., Hönisch, B., Miller, K.G, Rosenthal, Y., Wright, J. D.: Traditional and emerging geochemical proxies in foraminifera, J. Foraminifer. Res., 40, 165–192, https://doi.org/10.2113/gsjfr.40.2.165, 2010.

Lamy, F., Arz, H., Bond, G. C., Pätzold, J., and Bahr, A.: Multicentennial-scale hydrological changes in the Black Sea and northern Red Sea during the Holocene and the Arctic/North Atlantic Oscillation, Paleoceanography, 21, https://doi.org/10.1029/2005PA001184, 2006.

Laskar, J., Robutel, P., Joutel, F., Gastineau, M., Correia, A. C. M., and Levrard, B.: A long-term numerical solution for the insolation quantities of the Earth, Astron. Astrophys., 428, 261–285, https://doi.org/10.1051/0004-6361:20041335, 2004.

Locke, S., and Thunell, R. C.: Paleoceanographic record of the last glacial/interglacial cycle in the Red Sea and Gulf of Aden, Palaeogeogr., Palaeoclimatol., Palaeoecol., 64, 163–187, https://doi.org/10.1016/0031-0182(88)90005-3, 1988.

Lourens, L. J., Antonarakou, A., Hilgen, F. J., Van Hoof, A. A. M., Vergnaud-Grazzini, C., and Zachariasse, W. J.: Evaluation of the Plio-Pleistocene astronomical timescale, Paleoceanography, 11, 391–413, https://doi.org/10.1029/96PA01125, 1996.

500 Margreth, S., Rüggeberg, A., and Spezzaferri, S.: Benthic foraminifera as bioindicator for cold-water coral reef ecosystems along the Irish margin, Deep-Sea Research I, 56, 2216–2234, https://doi.org/10.1016/j.dsr.2009.07.009, 2009.

McCorkle, D. C., Keigwin, L. D., Corliss, B. H., and Emerson, S. R.: The influence of microhabitats on the carbon isotopic composition of deep-sea benthic foraminifera, Paleoceanography, 5, 161–185, https://doi.org/10.1029/PA005i002p00161, 1990.

505 McManus, J. F., Francois, R., Gherardi, J. M., Keigwin, L. D., and Brown-Leger, S.: Collapse and rapid resumption of Atlantic meridional circulation linked to deglacial climate changes, Nature, 428, 834–837, https://doi.org/10.1038/nature02494, 2004.

Müller, U.C., Pross, J., Tzedakis, P.C., Gamble, C., Kotthoff, U., Schmiedl, G., Wulf, S., Christanis, K.: The role of climate in the spread of modern humans into Europe. Quat. Sci. Rev., 30, 273-279, https://doi.org/10.1016/j.quascirev.2010.11.016,
510 2011.

Mulitza, S., Prange, M., Stuut, J. B., Zabel, M., von Dobeneck, T., Itambi, A. C., Nizou, J., Schulz, M., and Wefer, G.: Sahel megadroughts triggered by glacial slowdowns of Atlantic meridional overturning, Paleoceanography, 23, https://doi.org/10.1029/2008PA001637, 2008.

Murray, J.W.: Ecology and Applications of Benthic Foraminifera, Cambridge University Press, Cambridge, 426 pp.,
515 https://doi.org/10.1017/CBO9780511535529, 2006.

Naqvi, S. W. A., Hansen, H. P., and Kureishy, T. W.: Nutrient uptake and regeneration ratios in the Red Sea with reference to the nutrient budgets, Oceanol. Acta, 9, 271–275, https://archimer.ifremer.fr/doc/00110/22114/, 1986.

Niebler, H.-S.: Rekonstruktionen von Paläo-Umweltparametern anhand von stabilen Isotopen und Faunen-Vergesellschaftungen planktischer Foraminiferen im Südatlantik, Ber. Polarforschung, 167, 1–198, 1995.

520 North Greenland Ice Core Project members: High-resolution record of Northern Hemisphere climate extending into the last interglacial period, Nature, 31, 147–151, https://doi.org/10.1038/nature02805, 2004.

Papadopoulos, V. P., Zhan, P., Sofianos, S. S., Raitsos, D. E., Qurban, M., Abualnaja, Y., Bower, A., Kontoyiannis, H., Pavlidou, A., Asharaf, T. T. M., Zarokanellos, N., and Hoteit, I.: Factors governing the deep ventilation of the Red Sea, J. Geophys. Res.: Oceans, 120, 7493-7505, https://doi.org/10.1002/2015JC010996, 2015.

525 Raitsos, D. E., Pradhan, Y., Brewin, R. J. W., Stenchikov, G., and Hoteit, I.: Remote sensing the phytoplankton seasonal succession of the Red Sea, PLoS ONE, 8, e64909, https://doi.org/10.1371/journal.pone.0064909, 2013.

Rathburn, A. E., and Corliss, B. H., 1994. The ecology of living (stained) deep-sea benthic foraminifera from the Sulu Sea, Paleoceanography, 9, 87–150, https://doi.org/10.1029/93PA02327, 1994.

Rohling, E., and Cooke, S., Stable oxygen and carbon isotopes in foraminiferal carbonate shells. In: B.K. Sen Gupta (Ed.),
530 Modern Foraminifera. Kluwer Academic Publishers, Dordrecht/Boston/London, 239–258, 1999.

Rohling, E. J., Fenton, M., Jorissen, F. J., Bertrand, P., Ganssen, G., and Caulet, J. P.: Magnitudes of sea-level lowstands of the past 500,000 years, Nature, 394, 162–165, https://doi.org/10.1038/28134, 1998.

Field Code Changed

Rohling, E.J., Mayewski, P.A., Abu-Zied, R.H., Casford, J.S.L., Hayes, A.: Holocene atmosphere-ocean interactions: records from Greenland and the Aegean. Clim. Dyn., 18, 587-593, https://doi.org/10.1007/s00382-001-0194-8, 2002.Rohling, E. J., Marsh, R., Wells, N. C., Siddall, M., and Edwards, N. R.: Similar meltwater contributions to glacial sea level changes from Antarctic and northern ice sheets, Nature, 430, 1016–1021, https://doi.org/10.1038/nature02859, 2004.

Rohling, E. J., Grant, K., Hemleben, C., Kucera, M., Roberts, A. P., Schmeltzer, I., Schulz, H., Siccha, M., Siddall, M., and Trommer, G.: New constraints on the timing of sea level fluctuations during early to middle marine isotope stage 3, Paleoceanography, 23, https://doi.org/10.1029/2008PA001617, 2008.

Rohling, E. J., Grant, K., Bolshaw, M., Roberst, A. P., Siddall, M., Hemleben, C., and Kucera, M.: Antarctic temperature and global sea level closely coupled over the past five glacial cycles, Nat. Geosci., 2, 500–504, https://doi.org/10.1038/ngeo557, 2009.

Roman, R. E., and Lutjeharms, J. R. E.: Red Sea Intermediate Water in the source regions of the Agulhas Current, Deep-Sea Res. I, 56: 939–962, https://doi.org/10.1016/j.dsr.2009.01.003, 2009.

Rossignol-Strick, M.: African monsoons, an immediate climate response to orbital insolation, Nature, 304, 46–49, https://doi.org/10.1038/304046a0.

Schiebel, R., and Hemleben, C., Planktic foraminifers in the modern ocean, Springer, Berlin, Heidelberg, 358 pp., https://doi:10.1007/978-3-662-50297-6, 2017.

Schlitzer, R.: Data Analysis and Visualization with Ocean Data View, CMOS Bulletin SCMO 43, 9–13, 2015.

Schmelzer, I.: High-frequency event-stratigraphy and paleoceanography of the Red Sea, PhD thesis, Universiät Tübingen, Tübingen, 124 pp., 1998.

Schmiedl, G., and Mackensen, A.: Multispecies stable isotopes of benthic foraminifers reveal past changes of organic matter decomposition and deepwater oxygenation in the Arabian Sea. Palaeoceanography, 21, PA4213, https://doi.org/10.1029/2006PA001284, 2006.

Schmiedl, G., Pfeilsticker, M., Hemleben, C., and Mackensen, A.: Environmental and biological effects on the stable isotope composition of recent deep-sea benthic foraminifera from the western Mediterranean Sea, Mar. Micropaleontol., 51, 129–152, https://doi.org/10.1016/j.marmicro.2003.10.001, 2004.

Schulz, H., von Rad, U., and Erlenkeuser, H.: Correlation between Arabian Sea and Greenland climate oscillations of the past 110,000 years, Nature, 393, 54–57, https://doi.org/10.1038/31750, 1998.

Siddall, M., Rohling, E. J., Almogi-Labin, A., Hemleben, C., Meischner, D., Schmelzer, I., and Smeed, D. A.: Sea-level fluctuations during the last glacial cycle, Nature, 423, 853–858, https://doi.org/10.1038/nature01687, 2003.

Siddall, M., Rohling, E.J., Thompson, W.G., Waelbroeck, C.: Marine isotope stage 3 sea level fluctuations: Data synthesis and new outlook. Rev. Geophys., 46, RG4003, https://doi.org/10.1029/2007RG000226, 2008.

Siddall, M., Smeed, D. A., Hemleben, C., Rohling, E. J., Schmelzer, I., and Peltier, W. R.: Understanding the Red Sea response to sea level, Earth Planet. Sci. Lett., 225, 421–434, https://doi.org/10.1016/j.epsl.2004.06.008, 2004.

Sofianos, S. S., and Johns, W. E., 2007. Observations of the summer Red Sea circulation, J. Geophys. Res., 112, C06025, https://doi.org/10.1029/2006JC003886, 2007.

Smeed, D. A: Seasonal variation of the flow in the strait of Bah al Mandab, Oceanol. Acta, 20, 773–781, https://archimer.ifremer.fr/doc/00093/20433/, 1997.

Smeed, D. A.: Exchange through Bab el Mandab, Deep-Sea Res. II, 51: 455–474, https://doi.org/10.1016/j.dsr2.2003.11.002, 2004.

Svensson, A., Andersen, K. K., Bigler, M., Clausen, H. B., Dahl-Jensen, D., Davies, S. M., Johnsen, S. J., Muscheler, R., Parrenin, F., Rasmussen, S. O., Röthlisberger, R., Seierstad, I., Steffensen, J. P., and Vinther B. M.: A 60 000 year Greenland stratigraphic ice core chronology, Clim. Past, 4, 47–57, https://doi.org/10.5194/cp-4-47-2008, 2008.

Theodor, M., Schmiedl, G., and Mackensen, A.: Stable isotope composition of deep-sea benthic foraminifera under contrasting trophic conditions in the western Mediterranean Sea, Mar. Micropaleontol., 124, 16–28, https://doi.org/10.1016/j.marmicro.2016.02.001, 2016.

Thunell, R. C., Locke, S. M., and Williams, D. F.: Glacio-eustatic sea-level control on Red Sea salinity, Nature, 334, 601–604, https://doi.org/10.1038/334601a0, 1988.

Trommer, G., Siccha, M., Rohling, E. J., Grant, K., van der Meer, M. T. J., Schouten, S., Hemleben, C., Kucera, M.: Millennial-scale variability in Red Sea circulation in response to Holocene insolation forcing, Paleoceanography, 25, PA3203, https://doi10.1029/2009PA0011826, 2010.

Trommer, G., Siccha, M., Rohling, E. J., Grant, K., van der Meer, M. T. J., Schouten, S., Baranowski, U., Kucera, M.: Sensitivity of Red Sea circulation to sea level and insolation forcing during the last interglacial, Clim. Past, 7, 941–955, https://doi.org/10.5194/cp-7-941-2011, 2011

Vandenberghe, J., Renssen, H., van Huissteden, K., Nugteren, G., Konert, M., Lu, H., Dodonov, A., Buylaert, J.-P.: Penetration of Atlantic westerly winds into Central and East Asia, Quat. Sci. Rev., 25: 2380-2389, https://doi.org/10.1016/j.quascirev.2006.02.017, 2006.

Woelk, S., and Quadfasel, D.: Renewal of deep water in the Red Sea during 1982-1987, J. Geophys. Res., 101, 18155–18165, https://doi.org/10.1029/96JC01148, 1996.

Wolf, E. W., Chappellaz, J, Blunier, T., Rasmussen, S.O., Svensson, A.: Millennial-scale variability during the last glacial: The ice core record, Quat. Sci. Rev., 29, 2828–2838, https://doi:10.1016/j.quascirev.2009.10.013, 2010.